



Swansea University
Prifysgol Abertawe



Cronfa - Swansea University Open Access Repository

This is an author produced version of a paper published in :

Lubrication Science

Cronfa URL for this paper:

<http://cronfa.swan.ac.uk/Record/cronfa31547>

Paper:

Hill, D., Holliman, P., McGettrick, J., Searle, J., Appelman, M., Chatterjee, P., Watson, T. & Worsley, D. (2017).

Studies of inherent lubricity coatings for low surface roughness galvanised steel for automotive applications.

Lubrication Science

<http://dx.doi.org/10.1002/ls.1370>

This article is brought to you by Swansea University. Any person downloading material is agreeing to abide by the terms of the repository licence. Authors are personally responsible for adhering to publisher restrictions or conditions. When uploading content they are required to comply with their publisher agreement and the SHERPA RoMEO database to judge whether or not it is copyright safe to add this version of the paper to this repository.

<http://www.swansea.ac.uk/iss/researchsupport/cronfa-support/>

Studies of Inherent Lubricity Coatings for Low Surface Roughness Galvanized Steel for Automotive Applications

Journal:	<i>Lubrication Science</i>
Manuscript ID	LS-16-0083-RA-LS.R1
Wiley - Manuscript type:	Research Article - LS
Date Submitted by the Author:	n/a
Complete List of Authors:	Hill, Donald; Swansea University, Engineering Holliman, Peter; Bangor University, School of Chemistry McGettrick, James; Swansea University, Engineering Searle, Justin; Swansea University, Engineering Appleman, Marco; Tata Steel Research Development and Technology Chatterjee, Pranesh; Tata Steel Research Development and Technology Watson, Trystan; Swansea University, Engineering Wprsley, David; Swansea University, Engineering
Keywords:	
New Keyword Selection:	Coatings < Self-lubricating Materials < Lubricant Synthesis (Focus on Material), Solid Lubricants < Self-lubricating Materials < Lubricant Synthesis (Focus on Material), Chemical Analysis < Analysis < Lubricant Analysis and Diagnostics (Focus on Methods), Physical Analysis < Analysis < Lubricant Analysis and Diagnostics (Focus on Methods), Surface-sensitive Techniques < Tribo-chemistry < Lubrication Performance and Tribo-chemistry

SCHOLARONE™
Manuscripts

Studies of Inherent Lubricity Coatings for Low Surface Roughness Galvanized Steel for Automotive Applications

Donald Hill^a, Peter J. Holliman^{b,*}, James McGettrick^a, Justin Searle^a, Marco Appelman^c, Praneesh Chatterjee^c, Trystan M. Watson^a and David Worsley^a.

^a SPECIFC, College of Engineering, Swansea University, Baglan, Port Talbot, SA12 7AX, UK

^b School of Chemistry, Bangor University, Bangor, Gwynedd LL57 2UW, UK

^c TATA Research & Development 1970 CA IJmuiden

p.j.holliman@bangor.ac.uk

Sponsors

We gratefully acknowledge funding from EPSRC EngD and Tata Steel (DH), the Welsh Government for Sêr Cymru (PJH) and EPSRC/InnovateUK EP/I019278/1 (JMc, JS).

Abstract

Surface lubricity on TiO₂-coated galvanized steels can be controlled by solution depositing perfluorooctanoic (C8), lauric (C12) or stearic (C18) acids to avoid lubricating oils/emulsions or substrate pre-etching to remove surface oxide which add cost and waste. Water contact angles (WCA) reveal increased surface hydrophobicity on coated samples which correlate with linear friction testing (LFT) suggesting WCA can be used to screen lubricity compounds. LFT shows that C12 and C18 lower the coefficient of friction (μ) by 50-60% compared to uncoated substrates whilst C8 drops μ from 0.31 to 0.22. Surfaces have been characterized by XPS, SEM and AFM whilst IR confirms that as-deposited coatings contain physisorbed and deprotonated acids chemisorbed through esters and TGA confirms increasing loadings from C8 to C12 to C18. Surface washing removes physisorbed material and lowers μ by increasing surface organization and alkyl chain packing which enhances frictional energy dissipation through steric quenching.

Keywords: Lubricity; Friction; Sorption; Automotive steel; Sheet metal forming

1. Introduction

Galvanized steel is formed into complex shapes for vehicle bodies through techniques such as deep drawing which relies on material ductility to create new shapes as the substrate is forced over tools by the mechanical action of a punch^{1,2}. Adequate lubrication is essential to reduce friction to avoid wear on the substrate surface caused by frictional force at the interface between the substrate and the shaping tools³. Currently, drawing oils, emulsions or colloids are deposited onto automotive steels by spray, roll or drip coating to act as deep drawing lubricants⁴. Whilst these emulsions are non-toxic, they rely on the surface texture of the substrate to remain in place during

forming⁵. However, the poorer paint finish which can result from surface roughness⁶ means the automotive sector is increasingly driving towards smoother substrates.

Consequently, there is a need to develop alternative lubricants which can operate at a wider range of surface texture specifications of automotive steels. Conformal deposition at a molecular level avoids macro-surface roughness issues because it operates at an entirely different length scale (pm compared to μm). Previously, low surface energy monolayers have been used to generate low friction surfaces on different materials; e.g. stearate on Al⁷ or steel^{8,9}, silanes on Si¹⁰ or phosphonates on Cu¹¹. In general, the organic molecules that form such monolayers contain linker groups that bind to substrate surface atoms and alkyl chains that orient away from the surface to reduce interfacial shear forces¹². However, prior reports for the surface functionalize metals or metal oxides have often used pre-treatments such as polishing¹³ or plasma cleaning⁸ to generate homogeneous, ultra-clean and/or oxide-free surfaces. In a laboratory, these approaches work well but, on a production line, these extra steps increase cost and waste. Thus, we have taken the opposite approach and, rather than remove surface oxide, we have studied the self-assembly of carboxylic acids either onto pre-cast TiO₂ films or, where there is incomplete TiO₂ surface coverage, directly onto the native ZnO surface layer of galvanized steel. **We have chosen to use study the addition of a TiO₂ layer onto the galvanized substrate because** carboxylic acids have been observed to chemisorb as monolayers onto metal oxide surfaces (e.g. TiO₂) through ester linkages¹⁴⁻¹⁵ in a similar way to that used in dye-sensitized solar cells¹⁶⁻¹⁷.

In this paper, we report studies of using stearic, lauric or perfluorooctanoic acid to generate cost effective, low toxicity, processable films with controlled surface lubricity on low surface roughness, galvanized automotive steel. Whilst low friction, stearate films have been reported on Al⁷, steel^{8,9,13}, and mica¹⁹, to our knowledge, lauric and perfluorooctanoic acid have not been studied in this context. We have linked detailed characterization of these surfaces with coefficient of friction (μ) and contact angle data. Whilst correlations between atomic force microscopy friction coefficients and contact angle data have been reported for glass substrates¹⁸, we also report the first attempts to determine whether such a correlation exists for galvanized steel substrates as such correlation would enable contact angle measurements to be used as screening methods for compounds that could imbue surface lubricity.

2. Materials and Methods

2.1 Samples and chemicals

Galvanized steel (DX56, Tata Steel) was cut into 10×20 mm² coupons for characterization and 50×300 mm² strips for linear friction testing. The steel composition (% wt) was Al 0.036, C 0.0022, Mo 0.001, Ni 0.001, N 0.0035, P 0.009, Si 0.003, S 0.010, Sn 0.004, Ti 0.050, V 0.002, Cr 0.012, Cu 0.026, Mn 0.088, B 0.002 and the balance was Fe. The surface roughness was $0.97 \pm 0.05 \mu\text{m}$; measured using a Marsurf profilometer. All other chemicals were sourced from Sigma Aldrich and used without further purification.

2.2 Surface functionalization

Samples were air dried after each of the following steps. Surface oil was removed from the steel by scrubbing with water and detergent and then ultra-sonicating in acetone for 5min. Selected substrates were immersed in an isopropanolic solution of $\text{Ti}(\text{OPr})_4$ (10mM) for 30s. Substrates were then immersed in 100 mM isopropanolic solutions of the carboxylic acids for 30s before analysis. Selected samples were then either rinsed with acetone for 2 min or immersed in 100mM $\text{NaOH}_{(\text{aq})}$ for 30s.

2.3 Characterization

Contact angle measurements ($n = 5$, $5\mu\text{l}$ D.I. water) were made using the sessile drop technique with a USB 2.0 camera and goniometer and the data were fitted using FTA 32 software (FTA 32 Europe). IR spectra (4 scans, 4cm^{-1} resolution) were recorded on a Perkin Elmer 100 Series ATR-FTIR spectrometer, between 650 and 4000cm^{-1} . Field emission gun scanning electron microscopy (FEG-SEM) was carried out on a Hitachi S4800 at 1.0kV ($J_{\text{emission}} = 5\mu\text{A}$, working distance = 11.5mm). Energy dispersive X-Ray (EDX) spectra were recorded using a Silicon Drift X-Max EDX detector and Inca EDX software (Oxford Instr.) at 15.0kV ($J_{\text{emission}} = 15\mu\text{A}$, working distance = 17.0mm , acquisition = 100s). AFM data were measured over $10 \times 10 \mu\text{m}$ scan areas on a JPK Nanowizard 3 AFM in contact mode using a Si tip (thickness $3 \mu\text{m}$, length $225 \mu\text{m}$) with a force constant of 2.8N m^{-1} . The tip velocity was $20 \mu\text{m s}^{-1}$ with a line rate of 0.5Hz . X-Ray photoelectron spectra (XPS) were recorded on an Axis Supra XPS (Kratos Analytical) using a monochromated Al K_{α} source and large area slot mode detector ($300 \times 800\mu\text{m}$ analysis area). Data were recorded using a charge neutralizer to limit differential charging and binding energies were calibrated to the main hydrocarbon peak (BE 284.8eV). For each etch, a survey scan was recorded using a pass energy of 160eV . Data were fitted using CASA software with Shirley backgrounds. A 0.1eV step size was used when recording the high resolution spectra and a pass energy of 20eV . Thermal gravimetric analysis (TGA) data were recorded on a Pyris 1 TGA, heating from 25°C to 550°C at $25^{\circ}\text{Cmin}^{-1}$ under N_2 (20mlmin^{-1}). Coefficients of friction were measured using linear friction testing (LFT), a strip drawing test similar to that reported by Trzepiecinski *et al.*²⁰ at $22\text{-}24^{\circ}\text{C}$ and $30\text{-}45\%$ RH (ESI Fig. 1). To do this, samples ($50 \times 300\text{mm}$, $n = 3$) were pulled between round and cylindrical tools, clamped together with a force of 5kN , at 0.345mms^{-1} for a track length of 60mm . This sliding speed is slower than that typically used in deep drawing but was used to invoke very high friction to cause much faster removal of the zinc layer. Otherwise the tests would have required prohibitively very large amounts of material to study LFT. A new tool pair was used for each LFT test. The pulling force was measured and used to calculate the coefficient of friction (μ) by taking an average of the data between 40 and 50mm along the track length (where the values for μ had typically reached a plateau and where there is no longer believed to be any contribution from static friction behaviour which might occur at $< ca. 10 \text{mm}$) and using Eq. 1. All LFT tests were carried out in triplicate with mean values quoted (errors quoted are standard deviations from the mean).

$$\mu = \text{Pulling Force} / (2 \times \text{Normal Force}) \quad \text{Eq. 1}$$

Wear was assessed using digital photographs of the wear tools and by confocal microscopy using a Nanofocus μ Surf Mobile on 2.1mm x 2.1mm areas of steel samples at 20x magnification. The data were plotted using Mountains software, version 7.3.

3. Results and Discussion

3.1 Lubricity Compounds and Substrate

Lubricity compounds typically contain three main functionalities; a linker group to fix the compound to the substrate surface, a long (usually alkyl) chain which reduces surface energy and side groups attached to the long chain (Scheme 1a). In this work, three compounds have been studied all of which possess a carboxylic acid linker group. However, the compounds chosen vary in the length of alky chain and side groups they possess. Thus, perfluorooctanoic acid possesses only C-F side groups and consists of an 8 carbon chain and is subsequently labelled here as **C8**. By comparison, lauric and stearic acid possess only C-H side groups but consist of twelve and eighteen carbon chains and so are labelled here as **C12** and **C18**, respectively. The substrate chosen for lubricity testing (DX56) is galvanized steel with low surface roughness, which is designed for use in the automotive sector. The DX56 surface consists of a galvanic coating weight of 50-90 g m⁻² which corresponds to a thickness of *ca.* 9-13 μ m made up of 99.7 wt% Zn and 0.3 wt% Al. Thus, the outer surface of the DX56 substrate is expected to consist of a thin layer of predominantly ZnO.

Scheme 1 here

3.2 Infrared Spectroscopy

After removing surface oil from the DX56 substrate, the lubricity compounds have been deposited onto the steel by dip coating. IR data for **C8**-coated steel show a broad peak at *ca.* 3250cm⁻¹ (Fig. 1) which also appears in the spectrum of the neat acid (ESI Fig. 2). This is ascribed to inter-molecular H-bonding between the carboxylic acid moieties, suggesting there is physisorbed acid on the surface. However, the ν C=O of neat **C8** is not observed at 1711cm⁻¹ in the coated sample. Instead, two bands are observed at 1727 and 1652cm⁻¹ (Fig. 1), which are assigned as ν C=O and the asymmetric ν CO₂ of the carboxylate linker of **C8** bound to the oxide surface in the bridging coordination mode²¹. Bands at 1430 and 1366cm⁻¹ are assigned to the symmetric ν CO₂ of the bridging coordination mode and tentatively to the asymmetric ν CO₂ of carboxylates bound through monodentate coordination²¹. Whilst this suggests multiple coordination modes for **C8**, no bands for the monodentate carboxylate symmetric stretching vibration are observed.

Fig. 1 here

Previous studies have shown that carboxylic acids can chemisorb to metal oxide surfaces through covalent ester bonds^{7, 10, 21} and that physisorbed molecules can be

1
2
3 readily removed by solvent rinsing^{7, 8, 22}. To study this, acetone rinsing shows that,
4 whilst no carbonyl or carboxylate stretching bands are observed, ν C-F are present
5 between 1358 and 1140 cm^{-1} (ESI Fig. 3). This confirms that **C8** remains adsorbed and
6 suggests that the dipole moments of the carboxylate-related bands may be oscillating
7 parallel to the surface and so are invisible in the IR spectrum²³. Further evidence for this
8 is that, after $\text{NaOH}_{(\text{aq})}$ treatment to de-esterify the **C8**, there are no carboxylate or C-F
9 bands in the spectrum confirming that all the remaining **C8** has been desorbed (ESI
10 Fig. 4).
11

12
13 IR spectra for **C12**- and **C18**-coated DX56 show ν C-H at 3000-2800 cm^{-1} (Fig.
14 1). Both spectra show intense ν C=O bands at *ca.* 1700 cm^{-1} and weaker carboxylate
15 asymmetric ν CO₂ at *ca.* 1550 cm^{-1} whilst symmetric ν CO₂ bands are expected to be
16 coincident with carboxylate-related bands from physisorbed **C12** or **C18**. The signals
17 observed are ascribed to non-dissociated **C12** and **C18** acids along with surface-bound
18 esters^{7, 10, 13} suggesting that both of these coatings contain physi- and chemisorbed **C12**
19 and **C18**, respectively. For both acetone rinsed coatings, symmetric and asymmetric
20 ν CO₂ bands are observed at 1542 and 1400 cm^{-1} , respectively along with a band ascribed
21 to methylene scissoring at 1465 cm^{-1} ²⁴ (ESI Fig. 3). These bands confirm that esterified,
22 chemisorbed **C12** and **C18** remain on the surface whilst any physisorbed material is
23 removed. Analysis of $\Delta\nu$ between ν CO₂ *asym* and ν CO₂ *sym* gives a value of *ca.* 140 cm^{-1}
24 for **C12** and **C18** coatings which is consistent with carboxylate groups coordinating to
25 surface atoms in a bridging coordination mode²⁵. Such sorption has been observed in
26 prior studies whereby bonding proceeds through coordination of both carboxylate
27 oxygen atoms to two different surface sites^{4, 10, 22}. Scheme 1b shows bidentate
28 coordination of **C8**, **C12** and **C18** on a substrate surface.
29
30
31
32
33
34

3.3 Scanning Electron Microscopy (SEM)

35
36 SEM for “as received” DX56 steel shows contamination ascribed to oil deposited before
37 transit to minimize corrosion. After cleaning, SEM confirms oil removal (ESI Fig. 5a).
38 After dip coating DX56 in $\text{Ti}(\text{OiPr})_4$ solution, the surface topography reduces due to the
39 deposition of a TiO_2 film whilst EDX data confirms Ti is present (ESI Fig. 5b). For the
40 lubricity compounds, the **C8** surface shows few new features beyond the TiO_2 -coated
41 DX56 although the surface appears darker suggesting that the coating interacts
42 differently with the electron beam (Fig. 2a). The **C12** surface shows more surface
43 features suggesting a thicker film has been deposited (Fig. 2b) whilst the **C18** surface
44 shows needle-like structures (Fig. 2c) suggesting stearic acid has deposited as a separate
45 phase.
46
47
48

49 AFM data (ESI Fig. 7) of 10 x 10 μm areas of the samples show low surface
50 topography for the DX56 substrate (± 10 nm). After $\text{Ti}(\text{OPr})_4$ treatment, new features
51 are observed which are 200-250 nm in height and which are ascribed to TiO_2 particles
52 that we observe in the SEM. After deposition of **C8** (ESI Fig. 8), a much higher surface
53 topography is observed ($\pm 1,000$ nm) but this drops to ± 80 nm after rinsing in line with
54 removal of some physisorbed **C8**. However, the surface topography is still much greater
55 than the substrate suggesting that a model similar to Fig. 6d is occurring for **C8**. For the
56 **C12** surface, the surface topography is ± 200 nm but this drops to ± 10 nm barring
57
58
59
60

spikes for residual TiO₂ particles (ESI Fig. 9). However, the WCA remains hydrophobic and the coefficient of friction remains low. This suggests monolayer **C12** coverage represented in Fig. 6c. The as-deposited **C18** surface shows angular particles with surface topography ± 80 nm (ESI Fig. 10). XRD shows that these particles are crystalline indicating phase separation of excess stearate material (ESI Fig. 11). After acetone rinsing, these particles disappear but the surface topography (± 50 nm) suggests multiple layers of **C18** remain.

Fig. 2 here

3.4 X-ray photoelectron spectroscopy (XPS)

XPS data for cleaned DX56 show Zn 2p_{1/2} and Zn 2p_{3/2} photoelectron peaks at 1021.2 and 1044.0eV, respectively²⁶⁻²⁸ as well as a weak Al 2p photoelectron peak at 73.9eV (ESI Fig. 12 and 13). This is expected as Al is added to the galvanic Zn coating to control the structure of the intermetallic formed at the interface between the Zn coating and the underlying steel²⁶. A broad O 1s signal at 531.70eV also confirms the presence of surface oxide²⁶; mostly ZnO for the DX56 substrate. Fig. 3 shows that, after Ti(OiPr)₄ treatment, Ti 2p_{1/2} and Ti 2p_{3/2} peaks are observed at 458.0 and 463.7eV in agreement with previous studies²⁹⁻³¹. The O 1s signal also splits into two peaks at 531.2 and 529.5eV for ZnO and the newly formed TiO₂³².

TiO₂-coated DX56 treated with **C8** shows an intense F 1s photoelectron peak at 689.9eV (ESI Fig. 14) confirming the presence of fluorine on the surface³³. A C 1s peak centred at *ca.* 291.8eV de-convolutes to reveal the presence of C=O, CF₂, and CF₃ moieties for the fluorinated carboxylic acid³⁴ (Fig. 3). For the TiO₂-coated DX56 treated with **C12** or **C18**, the C 1s peak envelopes de-convolutes to reveal the presence C=O, C-CO₂ and C-C components (Fig. 3) as expected for these alkyl carboxylates. The assignments are in line with related studies for carboxylic acids binding to steel¹³ or iron oxide surfaces¹⁰.

As a way to compare the loadings of **C8**, **C12** and **C18**, the at% of C 1s was found to be 31.6%, 66.4% and 91.7%, respectively. In this context, for typical photoelectron kinetic energies (10-1000eV), mean free path escape depths are 1-10nm corresponding to 2-10 monolayers³⁵. Thus the lower at% of carbon and the higher intensity Zn 2p peaks for **C8** (3.7 at% Zn) suggest either poor coverage with substantial surface area not occupied by **C8** and/or a **C8** loading of 1-2 monolayers. For **C12**, the at% of C more than doubles whilst the Zn drops accordingly (1.2 at% Zn) suggesting either a higher coverage of **C12** and/or a multilayer **C12** loading. By comparison, the **C18** coating shows the highest at% for C along with the lowest intensity Zn 2p peaks (0.2 at% Zn) which suggests almost complete coverage of **C18** on the surface and/or a many multilayer loading of **C18**. To further understand loadings on TiO₂ surfaces, **C8**, **C12** or **C18** were sorbed onto Degussa P25 powder and then thermal gravimetric analysis (TGA) was measured to study the mass loss following their combustion (ESI Fig. 15 and ESI Table 1). From these data, the mass of **C8**, **C12** or **C18** initially sorbed onto P25 was found to be 10.9%, 71.0% and 78.8%, respectively. After acetone washing, the sorbed masses of C8, C12 or C18 drop to 8.7%, 24.9% and 44.5%,

1
2
3 respectively. Whilst these data show very little change in the **C8** loading after washing,
4 the **C12** loading drops by almost two-thirds and **C18** drops by almost a half. These data
5 correlate strongly with the IR data which lower peak intensities for the lubricity
6 compounds (**C8**, **C12** or **C18**) spectra after acetone washing.
7

8 Assuming 10mg of coated P25 TiO₂, the acetone-washed loadings correspond to
9 2.1μmoles, 12.4μmoles and 15.6μmoles of **C8**, **C12** or **C18**. Given that P25 has a
10 surface area of *ca.* 50m²g⁻¹¹⁵, a 10mg sample has a surface area of 0.5m². The cross-
11 sectional area of **C18** have been reported to be 20.7Å²³⁶. Thus, to form a monolayer of
12 **C18** on 10mg of P25 should require 4.0μmole of **C18**. Given that **C8** and **C12** both
13 possess a similar carboxylate linkers to **C18**, it can be assumed that their cross-sectional
14 areas should also be similar and thus should require similar loadings to achieve
15 monolayer coverage. Thus, these data suggest an average of *ca.* 0.5, 3.0 and 4.0
16 monolayer coverage for **C8**, **C12** and **C18**, respectively.
17
18
19

20
21 **Fig. 3 here**
22

23 **3.5 Water contact angle measurements**

24 The water contact angle (WCA) of “as received” DX56 galvanized steel were highly
25 variable, which is ascribed to surface oil used to reduce corrosion in transit. After
26 thorough cleaning, DX56 displays a more consistent WCA (55 ± 5°) (Fig. 4). Whilst the
27 WCA did not vary after Ti(OiPr)₄ treatment, the addition of either **C12** or **C18**
28 generates hydrophobic surfaces with WCA of 88 ± 3° and 110 ± 8° respectively
29 suggesting these surfaces have been covered by the carboxylic acids. Similar WCA
30 values have been reported for alkythiols on gold³⁷, alkylsilanes on paper³⁸ and
31 carboxylic acids on mica³⁹. By comparison, the equivalent **C8** samples display
32 hydrophilic WCA similar to the TiO₂-coated and uncoated DX56 (58 ± 7°). This may be
33 due to lower or less homogeneous **C8** surface coverage or potentially the formation of a
34 **C8** bi-layer whereby a second layer of **C8** molecules orient their carboxylic acid groups
35 away from the surface, increasing interaction with droplet water molecules (Fig. 6d).
36 However, the TGA data for **C8** adsorbed onto P25 TiO₂ show only 0.5 monolayer
37 loading which suggests low coverage is the main reason for the low WCA value. To test
38 this further, the WCA of acetone rinsed samples were also measured to ensure the
39 removal of any physisorbed **C8**, **C12** or **C18**.
40
41
42
43
44

45 As expected, acetone rinsing did not affect the WCA of DX56 or TiO₂-coated
46 DX56. However, acetone rinsing **C8**-coated samples does increase WCA to 75 ± 6°,
47 suggesting more of the surface consists of C-F terminated chains. Similarly, the WCA
48 of **C12** increases to 108 ± 6° in line with a more hydrophobic surface. In this case,
49 removing physisorbed **C12** increases the proportion of the surface which is C-H alkyl
50 terminated. Finally, rinsing **C18**-coated samples does not change the WCA which
51 suggests that, prior to rinsing, the surface was already alkyl terminated (Fig. 6d).
52
53
54

55 **Fig. 4 here**
56

57 **3.6 Linear Friction Testing (LFT)**

Coefficients of friction (μ) have been determined using LFT which is an aggressive tribological test, during which the galvanized coating is completely removed (Fig. 5a). Fig. 5b shows how μ varies along the samples. Cleaned DX56 shows the highest friction during the first 10mm ($\mu > 0.35$), which then drops to between $\mu = 0.22-0.30$. The initial increased friction observed may be due to several reasons including stick-slip behaviour resulting from substantial differences in roughness across the substrate surface, running in behaviour being influenced by surface roughness, the presence of a built-up transfer layer or adhesive friction between the tool and substrate. The dynamic value of μ (0.23) for TiO₂-coated DX56 suggests that adding TiO₂ to the surface does not influence lubricity. For the coated samples, μ displays little variation along the samples and this absence of variable friction behaviour suggests that surface coverage is sufficiently homogeneous to overcome substrate surface roughness.

Interestingly, the C8 coating displays a dynamic μ of 0.20, which remains the same after acetone rinsing (Fig. 5c). The high friction observed is in agreement with previous studies; high μ values have also been observed for perfluorinated carboxylic acids on silicon⁴⁰ and for perfluorinated phosphonates on copper¹¹. High μ values have also been observed on related systems involving fluorinated⁴¹ or perfluorinated^{11, 40} monolayers; discussions in the literature have attributed this to a number of factors including lower packing densities, relative to their hydrocarbon analogues, the molecular size of terminal groups, and molecular disorder in the molecular films⁴². By comparison, the C12 and C18 coatings give μ values of 0.11 and 0.10 (Fig. 5c). This is in agreement with previously reported studies where large reductions in μ values have been reported for phosphonates on copper¹¹, silanes on silicon¹⁰, and carboxylic acids on Al⁷ and steel⁹, wherein it is believed that energy dissipation occurs through steric quenching between neighbouring alkyl chains⁴³. After acetone rinsing, the dynamic μ of C12 and C18 coatings remain the same suggesting that sufficient chemisorbed material remains to imbue lubricity to these surfaces. Prior studies have shown that the stabilization energy incurred through increasing the number (n) of methylene (CH₂) groups in a chain saturates between n = 8-10⁴³.

Analysis of the wear tools using digital photography (ESI Fig. 16) shows that, after LFT testing, there is less build-up of larger zinc flakes on the wear tools that had been used to test the C12 and C18 coatings compared to the uncoated FF substrate which is in agreement with the LFT data that these coatings reduce the coefficient of friction for these samples. Also in line with the wear tool imaging and LFT data, confocal microscopy (ESI Fig. 17) shows smaller scratches for the C12 and C18 coatings which suggests that less material has been removed and hence that the wear is lower for these coatings.

A plot of μ vs WCA (Fig. 6a) shows that a negative correlation exists between the coefficient of friction and surface wettability. This suggests that it should be possible to predict substrate lubricity from contact angle data because, whilst WCA data only provide averaged information across the surface area of the water droplet used, these data do provide a measure of the extent of functionalization of surfaces. This is key because it has been reported that close-packed monolayers can facilitate low friction behaviour on some surfaces by enabling energy dissipation by steric quenching

1
2
3 between neighbouring alkyl chains during tribological contact⁴³. Thus, whilst the
4 correlation between WCA and μ effectively reflects surface coverage, the observed
5 trend cannot take into account multiple layers and/or the molecular orientation within
6 the surface films. However, with these provisos, our data do show that WCA can be
7 used as a rapid screening method to identify substrate friction properties.
8

9 Applying this to our samples, for **C8** this explains the high value of μ because
10 the low surface coverage of **C8** reduces inter-molecular steric quenching whilst
11 uncoated areas possess no effective barrier during sliding (Fig. 6c). By comparison,
12 SEM and XPS data for the unrinsed **C12** and **C18** samples, show that the films are
13 thicker than **C8**, show higher surface coverage and contain both physisorbed carboxylic
14 acids and chemisorbed carboxylates (Fig. 6c,d). Therefore, it is plausible to suggest that,
15 prior to rinsing, the films act as more like barrier coatings, preventing interfacial contact
16 between the substrate and tool during tribological contact. Interestingly, μ does not vary
17 for these samples after solvent rinsing even though IR data shows that only
18 chemisorbed carboxylates remain on the surface. This can be ascribed to the
19 chemisorbed **C12** and **C18** carboxylates forming more ordered films where the alkyl
20 chains are sufficiently ordered and close packed to enable steric quenching between
21 neighbouring chains and thus to reduce frictional forces. This model for the structures
22 of the coatings is shown (Fig. 6b-d). This shows that the TiO₂ layer formed as a result
23 of dip coating process produces a partially covered surface. Between the TiO₂-rich areas
24 is ZnO from oxidation of the Zn-rich galvanic layer. Where metal oxide is present, the
25 carboxylic acids can then chemisorb through esterification to surface hydroxide groups
26 to form a monolayer where the alkyl groups orient themselves away from the substrate
27 surface. However, if the loading is high enough, additional layers can physisorb as
28 shown in Fig. 6d. Where free carboxylic acid groups orient themselves away from the
29 substrate surface, it is possible for this to lower the WCA and increase μ . Whilst solvent
30 rinsing can remove this physisorbed material, only de-esterification using strong base
31 can remove the chemisorbed species.
32
33
34
35
36
37
38
39

40 **Fig. 5 here**

41 **4. Conclusions**

42 Controlling surface lubricity is key for reducing wear during metal forming. At the
43 same time, reducing waste and improving surface finish are driving the need to avoid
44 oil-based lubrication and to reduce the substrate surface roughness required for such
45 emulsions to work. Our approach to these problems has been to develop films which
46 imbue inherent lubricity to metal surfaces. Whilst previous reports have suggested this
47 is possible by pre-etching the substrate to remove surface oxide, we have instead
48 attached monolayers of oriented alkyl chains directly to the oxide surface through
49 carboxylate linkers. This approach is both cost effective and scaleable and we have used
50 it on substrates up to 30cm in dimension. We have also screened different alkyl chain
51 lengths and side groups (C-F vs C-H) and found that the initial deposits are thicker,
52 multi-layer films but that acetone washing removes physisorbed material for all the
53 compounds tested. However, **C12** (lauric acid) is the most effective in terms of
54
55
56
57
58
59
60

monolayer coverage, WCA and coefficient of friction. By comparison, **C8** (octanoic acid) shows low WCA and high μ whilst, for **C18** (stearic acid), phase-separated particles of **C18** are observed but, even after acetone rinsing, there is still too much material resulting in multi-layer surface films. Whilst stearic acid is not expensive this is still inefficient and wastes material. Through analysis of these data, it was also found that water contact angles can act as an effective screening method for compounds that could increase the surface lubricity.

Fig. 6 here

References

1. Allen SJ, Mahdavian SM, The effect of lubrication on die expansion during the deep drawing of axisymmetrical steel cups, *J. Mater. Process. Tech.*, 2008; **199**: 102-107. DOI:10.1016/j.jmatprotec.2007.08.005.
2. Abe Y, Ohmi T, Mori K, Masuda T, Improvement of formability in deep drawing of ultra-high strength steel sheets by coating of die, *J. Mater. Process. Tech.*, 2014; **214**: 1838-1843. DOI:10.1016/j.jmatprotec.2014.03.023.
3. Stepina V, Vesely V, in *Lubricants and Special Fluids*, Elsevier, Amsterdam, 1992, 2.
4. Lascoe OD, in *Handbook of Fabrication Processes*, 5th Ed., 1988, ASM Int., 264.
5. Oberg E, Jones FD, Horton HL, Ryffel HH, in *Machinery's Handbook*, 29th Ed., 2012, Ind. Press, NY, 1372.
6. Davies G, in *Materials for Automobile Bodies*, Elsevier, Oxf., 2012, 113.
7. Zhang Q, Wan Y, Li Y, Yang S, Yao W, Friction reducing behavior of steric acid on a textured aluminium substrate, *Appl. Surf. Sci.*, 2013; **280**: 545-549. DOI: 10.1016/j.apsusc.2013.05.024
8. Ruths M, Lundgren S, Danerlöv K, Persson K, Friction of fatty acids in nanometer-sized contacts of different adhesive strength, *Langmuir*, 2008; **24**: 1509-1516. DOI: 10.1021/la7023633.
9. Loehlé S, Matta C, Minfray C, Le Mogne T, Iovine R, Obara Y, Miyamoto A, Martin JM, Mixed lubrication of steel by C18 fatty acids revisited. Part I: toward the formation of carboxylate, *Tribol. Int.*, 2015; **82**: 218-227. DOI: 10.1016/j.triboint.2015.08.036.
10. De Palma V, Tillman N, Friction and wear of self-assembled trichlorosilane monolayer films on silicon, *Langmuir*, 1989; **5**: 868-872. DOI: 10.1021/la00087a049
11. Hoque E, DeRose JA, Bhushan B, Hipps KW, Low adhesion, non-wetting phosphonate self-assembled monolayer films formed on copper oxide surfaces, *Ultramicroscopy*, 2009; **109**: 1015-1022. DOI: 10.1016/j.ultramic.2009.03.033
12. Liu H, Bhushan B, Investigation of nanotribological properties of self-assembled monolayers with alkyl and biphenyl spacers, *Ultramicroscopy*, 2002, **91**: 185-202. DOI: 10.1016/S0304-3991(02)00099-2.

- 1
2
3 13. Sahoo RR, Biswas SK, Frictional response of fatty acids on steel, *J. Colloid*
4 *Interface Sci.*, 2009; **333**:707-718. DOI: 10.1016/j.jcis.2009.01.046.
5
6 14. Holliman PJ, Vaca Velasco B, Butler I, Wijdekop M, Worsley D, Studies of dye
7 sensitisation kinetics and sorption isotherms of Direct Red 23 on titania. *Int. J.*
8 *Photoenergy*, 2008; 1-8. DOI: 10.1155/2008/827605.
9
10 15. Charbonneau C, Holliman PJ, Davies M, Watson T, Worsley D, Facile self-
11 assembly and stabilization of metal oxide nanoparticles, *J. Colloid Interface Sci.*,
12 2015; **442**: 110-119. DOI: 10.1016/j.jcis.2014.11.042.
13
14 16. Holliman PJ, Al-Salihi KJ, Connell A, Davies ML, Jones EW, Worsley DA,
15 Development of selective, ultra-fast multiple co-sensitization to control dye loading
16 in dye-sensitized solar cells, *RSC Adv.*, 2014; **4**: 2515-2522. DOI:
17 10.1039/c3ra42131g
18
19 17. Connell A, Holliman PJ, Jones EW, Furnell L, Kershaw C, Davies ML, Gwenin
20 CD, Pitak MB, Coles SJ, Cooke G, Multiple linker half-squarylium dyes for dye-
21 sensitized solar cells; are two linkers better than one? *J. Mater. Chem. A*, 2015; **3**;
22 2883-2894. DOI: 10.1039/C4TA06896C
23
24 18. Beake BD, Leggett GJ, Variation on frictional forces in air with the composition of
25 heterogeneous organic surfaces, *Langmuir*, 2000; **16**: 735-739. DOI:
26 10.1021/la990782d
27
28 19. Lundgren SM, Ruths M, Danerlöv K, Persson K, Effects of unsaturation on film
29 structure and friction of fatty acids in a model base oil, *J. Colloid Interface Sci.*,
30 2008; **326**: 530-536. DOI: 10.1016/j.jcis.2008.05.068
31
32 20. Trzpiecinski T, Bazan A, Lemu HG, Frictional characteristics of steel sheets used
33 in automotive industry, *Int. J. Automotive Tech.*, 2015; **16**: 849-863. DOI:
34 10.1007/s12239-015-0087-1
35
36 21. Przedlacki M, Kajdas C, Tribochemistry of fluorinated fluids hydroxyl groups on
37 steel and aluminium surfaces, *Tribol. Trans.*, 2006; **49**: 202-214. DOI:
38 10.1080/05698190500544676
39
40 22. Taheri P, Wielant J, Hauffman T, Flores JR, Hannour F, de Wit JHW, Mol JMC,
41 Terryn H, A comparison of the interfacial bonding properties of carboxylic acid
42 functional groups on zinc and iron substrates, *Electrochim. Acta*, 2011; **56**: 1904-
43 1911. DOI: 10.1016/j.electacta.2010.10.079
44
45 23. Greenler RG, Snider DR, Witt D, Sorbello RS, The metal-surface selection rule for
46 infrared spectra of molecules adsorbed on small metal particles, *Surf. Sci.*, 1982,
47 **118**: 415-428. DOI: 10.1016/0039-6028(82)90197-2
48
49 24. Ozturk S, Balkose D, Okur S, Umemura J, Effect of humidity on electrical
50 conductivity of zinc stearate nanofilms, *Colloids Surf. A: Physicochem. Eng.*
51 *Aspects*, 2007; **302**: 67-74. DOI: 10.1016/j.colsurfa.2007.01.039.
52
53 25. Kutscher JS, Gericke A, Hühnerfuss H, Effect of bivalent Ba, Cu, Ni and Zn cations
54 on the structure of octadecanoic acid monolayers at the air-water interface as
55 determined by external infrared reflection-absorption spectroscopy, *Langmuir*,
56 1996; **12**: 1027-1034. DOI: 10.1021/la950731q.
57
58
59
60

- 1
2
3 26. Feliu Jr. S, Barranco V, XPS study of the surface chemistry of conventional hot-dip
4 galvanized pure Zn, galvanneal and the Zn-Al alloy coatings on steel, *Acta*
5 *Materialia*, 2003; **51**: 5413-5424. DOI: 10.1016/S1359-6454(03)00408-7
6
7 27. Lebrini M, Fontaine G, Gengembre L, Traisnel M, Lerasle O, Genet N, Corrosion
8 behaviour of galvanized steel and electroplating steel in aqueous solution: AC
9 impedance study and XPS, *Appl. Surf. Sci.*, 2008; **254**: 6943-6947. DOI:
10 10.1016/j.apsusc.2008.04.112
11
12 28. Arenas MA, García I, Damborenea J, X-ray photoelectron spectroscopy study of the
13 corrosion behaviour of galvanised steel implanted with rare earths, *Corrosion Sci.*,
14 2004; **46**:1033-1049. DOI: 10.1016/S0010-938X(03)00193-8
15
16 29. Pazokifard S, Farrokhpay S, Mirabedini M, Esfandeh M, Surface treatment of TiO₂
17 nanoparticles via sol-gel method: effect of silane type on the hydrophobicity of the
18 nanoparticles, *Progr. Org. Coatings*, 2015; **87**: 36-44. DOI:
19 10.1016/j.porgcoat.2015.04.021
20
21 30. Al-Kandari H, Mohamed AM, Al-Kharafi F, Katrib A, XPS-UPS, ISS
22 characterization studies and the effect of Pt and K addition on the catalytic
23 properties of MoO_{2-x}(OH)_y deposited on TiO₂, *J. Electron Spec. Related Phenom.*,
24 2011; **184**: 472-478. DOI: 10.1016/j.elspec.2011.07.001.
25
26 31. Kruse N, Chenakin S, XPS characterization of Au/TiO₂ catalysts: binding energy
27 assessment and irradiation effects, *Appl. Catal. A: Gen.*, 2011; **391**: 367-376. DOI:
28 10.1016/j.apcata.2010.05.039.
29
30 32. Hanawa T, Ota M, Calcium phosphate naturally formed on titanium in electrolyte
31 solution, *Biomater.*, 1991; **12**: 767-774. DOI: 10.1016/0142-9612(91)90028-9
32
33 33. Beamson G, Briggs D, High Resolution XPS of Organic Polymers ESCA300
34 Database, 1992.
35
36 34. Suzuki S, Whittaker MR, Wentrup-Byrne E, Monterio MJ, L. Grondahl L,
37 Adsorption of well-defined fluorine-containing polymers onto
38 poly(tetrafluoroethylene), *Langmuir*, 2008; **24**: 13075-13083. DOI:
39 10.1021/la802300q
40
41 35. Seah MP, Dench WA, Quantitative electron spectroscopy of surfaces: a standard
42 database for electron inelastic mean free paths in solids, *Surf. Interface Anal.*, 1979;
43 **1**: 2-11. DOI: 10.1002/sia.740010103
44
45 36. Lane CL, Burton E, Crabb CC, Accurate molecular dimensions from stearic acid
46 monolayers, *J. Chem. Ed.*, 1984; **61**: 815. DOI: 10.1021/ed061p815
47
48 37. Nuzzo RG, Allara DL, Adsorption of bifunctional organic disulfides on gold
49 surfaces, *J. Am. Chem. Soc.*, 1983; **105**: 4481-4483. DOI: 10.1021/ja00351a063
50
51 38. Oh MJ, Lee SY, Paik KH, Preparation of hydrophobic self-assembled monolayers
52 on paper surfaces with silanes, *J. Ind. Eng. Chem.*, 2011; **17**: 149-153. DOI:
53 10.1016/j.jiec.2010.12.014.
54
55 39. Sauthiera G, Segurac JJ, Fraxedasa J, A. Verdaguer A, Hydrophobic coatings of
56 mica by stearic acid vapor deposition, *Colloids Surf. A: Physicochem. Eng. Aspects*,
57 2014; **443**: 331-337. DOI: 10.1016/j.colsurfa.2013.11.031.
58
59
60

- 1
2
3 40. Singh RA, Yoon ES, Han HG, Kong H, Friction behaviour of chemical vapor
4 deposited self-assembled monolayers on silicon wafer, *Wear*, 2007; **262**: 130-137.
5 DOI: 10.1016/j.wear.2006.04.001.
6
7 41. Kim HI, Graupe M, Oloba O, Koini T, Imaduddin S, Lee TR, Perry SS, Molecularly
8 specific studies of the frictional properties of monolayer films: a systematic
9 comparison of CF₃-, (CH₃)₂CH-, and CH₃-terminated films, *Langmuir*, 1999; **15**:
10 3179-3185. DOI: 10.1021/la981497h.
11
12 42. Singh RA, Kim J, Yang SW, Oh JE, Yoon ES, Tribological properties of
13 trichlorosilane-based one- and two-component self-assembled monolayers, *Wear*,
14 2008; **265**: 42-48. DOI: 10.1016/j.wear.2007.08.016.
15
16 43. Lio A, Charych DH, Salmeron M, Comparative atomic force microscopy study of
17 the chain length dependence of frictional properties of alkanethiols on gold and
18 alkylsilanes on mica, *J. Phys. Chem. B*, 1997; **101**: 3800-3805. DOI:
19 10.1021/jp963918e
20
21
22
23
24
25
26
27
28
29
30
31
32
33
34
35
36
37
38
39

40 List of Schemes and Figures

41
42 **Scheme 1** Schematic of **C18** (top), **C12** (middle) or **C8** (bottom) bound to surface sites
43 in bridging coordination mode. H atoms omitted for clarity.
44

45
46 **Fig. 1** Infrared spectra of DX56 steel treated with (a) **C8** (b) **C12** or (c) **C18**.

47 ● νC-H, ♣ νO-H, ▼ νC=O, † ν CO₂ asym bridge, γ νCO₂ sym bridge, ‡ νCO₂ asym mon, α νC-F
48
49

50 **Fig. 2** SEM data for TiO₂-coated DX56 steel treated with (a) **C8**, (b) **C12** or (c) **C18**.
51

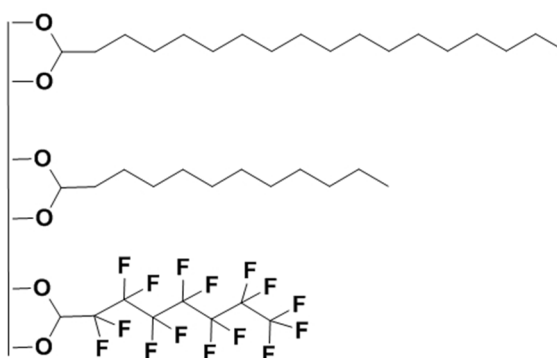
52
53 **Fig. 3** High resolution XPS spectra of TiO₂-coated DX56 substrate (a) Ti 2p and (b) O
54 1s are regions. Other spectra show C 1s regions after treatment with (c) **C8** or (d) **C12**.
55 C=O (▼), C-CO₂ (◆), C-C (‡), CF₃ (■), CF₂ (●), COO (†), C-O (♣).
56
57
58
59
60

1
2
3 **Fig. 4** (a) contact angles before (dark) and after (light) acetone rinsing and images for
4 (b) TiO₂-coated DX56 and TiO₂-coated DX56 with (c) **C8**, (d) **C12** and (e) **C18**.
5
6

7 **Fig. 5** (a) Image of sample after linear friction testing (LFT), (b) dynamic coefficient of
8 friction (μ) data and (c) mean μ for substrates before (dark shading) or after (light
9 shading) acetone rinsing. DX56 steel (grey), TiO₂-coated DX56 (black) and DX56
10 coated with **C12** (circles), **C18** (hashed) and **C8** (light grey).
11
12

13 **Fig. 6** (a) Data for μ versus contact angle for DX56 steel (grey), TiO₂-coated DX56
14 steel (black), and DX56 steel with **C12** (dotted), **C18** (hashed) and **C8** (open). Circles
15 are before acetone rinsing and triangles are after acetone rinsing, (b) schematic of
16 lubricity compound, and proposed models for (c) monolayer and (d) multilayer coatings
17 of carboxylic acids on DX56 steel.
18
19
20
21
22
23
24
25
26
27
28
29
30
31
32
33
34
35
36
37
38
39
40
41
42
43
44
45
46
47
48
49
50
51
52
53
54
55
56
57
58
59
60

Holliman Scheme 1



Scheme 1 Schematic of C18 (top), C12 (middle) or C8 (bottom) bound to surface sites in bridging coordination mode. H atoms omitted for clarity.

Scheme 1 here
190x275mm (96 x 96 DPI)

Holliman Fig. 1

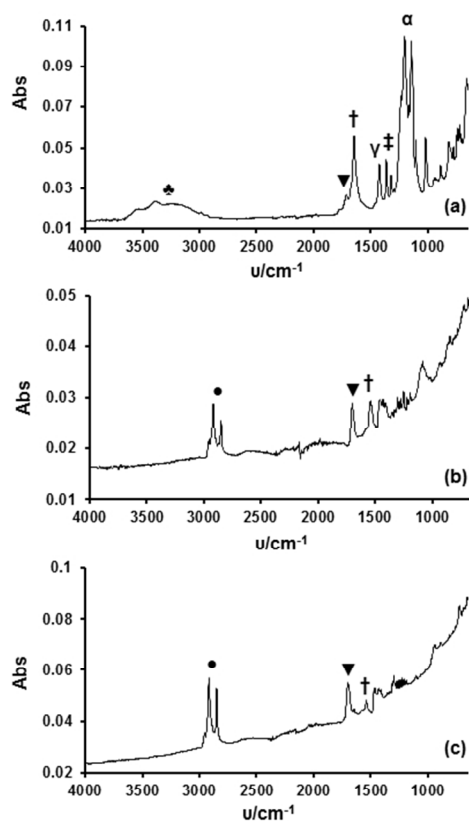


Fig. 1 Infrared spectra of DX56 steel treated with (a) C8 (b) C12 or (c) C18.
 • ν C-H, ♣ ν O-H, ▼ ν C=O, † ν CO₂ asym bridge, γ ν CO₂ sym bridge, ‡ ν CO₂ asym mon, α ν C-F

Fig. 1 here
 190x275mm (96 x 96 DPI)

Holliman Fig. 2

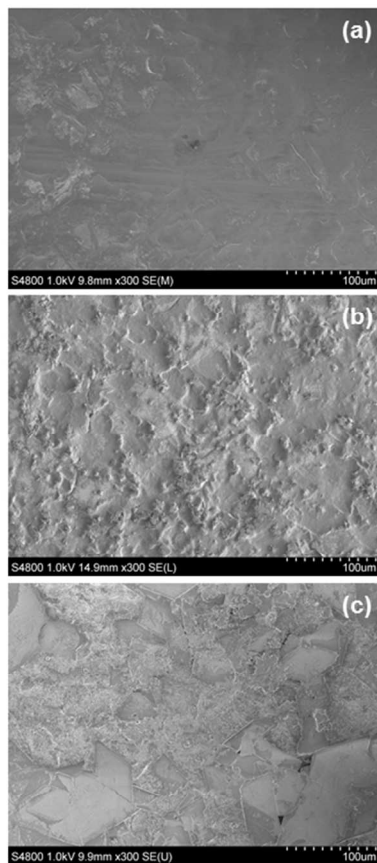


Fig. 2 SEM data for TiO₂-coated DX56 steel treated with (a) C8, (b) C12 or (c) C18.

Fig. 2 here

190x275mm (96 x 96 DPI)

Holliman Fig. 3

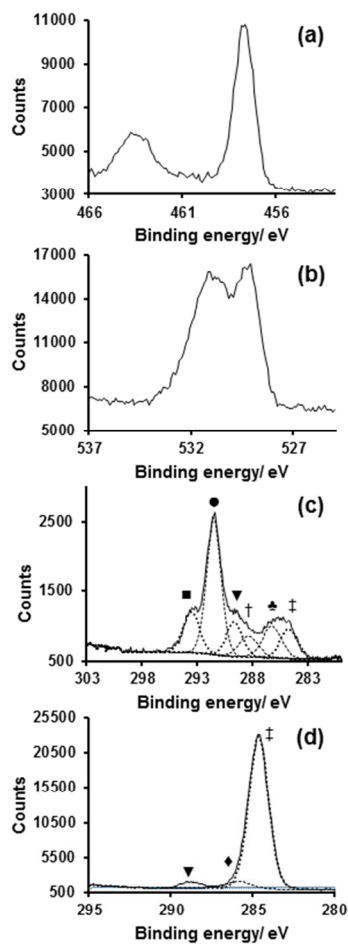


Fig. 3 High resolution XPS spectra of TiO₂-coated DX56 substrate (a) Ti 2p and (b) O 1s are regions. Other spectra show C 1s regions after treatment with (c) C8 or (d) C12. C=O (▼), C-CO₂ (◆), C-C (‡), CF₃ (■), CF₂ (●), COO (†), C-O (♣).

Fig. 3 here

190x275mm (96 x 96 DPI)

Holliman Fig. 4

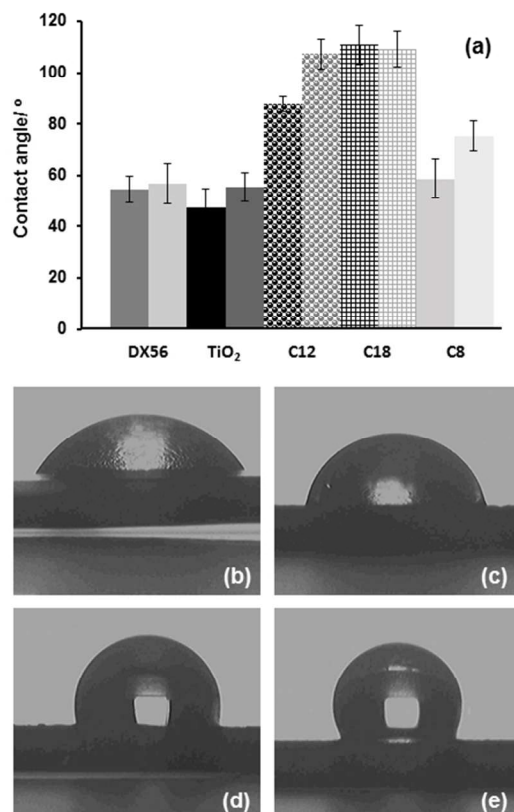


Fig. 4 (a) contact angles before (dark) and after (light) acetone rinsing and images for (b) TiO₂-coated DX56 and TiO₂-coated DX56 with (c) C8, (d) C12 and (e) C18.

Fig. 4 here

190x275mm (96 x 96 DPI)

Holliman Fig. 5

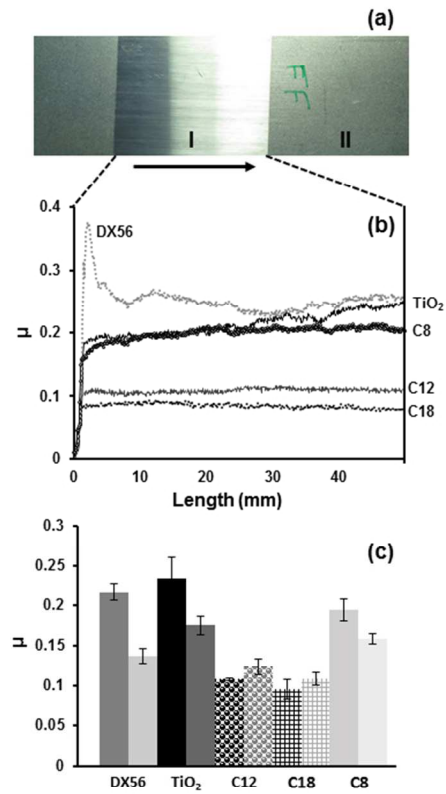


Fig. 5 (a) Image of sample after linear friction testing (LFT), (b) dynamic coefficient of friction (μ) data and (c) mean μ for substrates before (dark shading) or after (light shading) acetone rinsing. DX56 steel (grey), TiO₂-coated DX56 (black) and DX56 coated with C12 (circles), C18 (hashed) and C8 (light grey).

Fig. 5 here

190x275mm (96 x 96 DPI)

Holliman Fig. 6

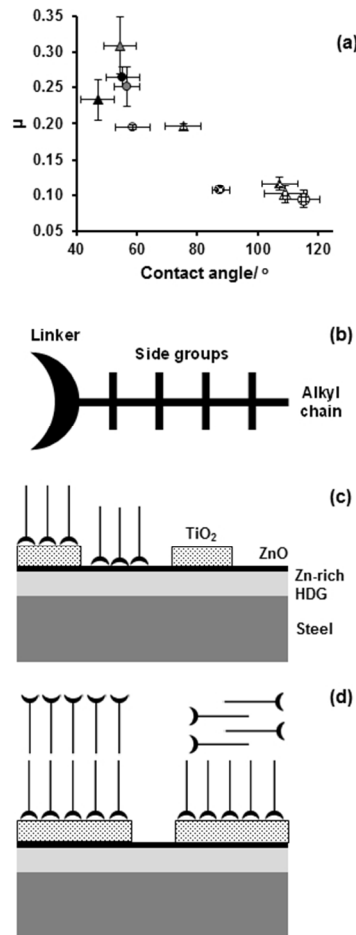


Fig. 6 (a) Data for μ versus contact angle for DX56 steel (grey), TiO₂-coated DX56 steel (black), and DX56 steel with C12 (dotted), C18 (hashed) and C8 (open). Circles are before acetone rinsing and triangles are after acetone rinsing, (b) schematic of lubricity compound, and proposed models for (c) monolayer and (d) multilayer coatings of carboxylic acids on DX56 steel.

Fig. 6 here
190x275mm (96 x 96 DPI)